

## Article

**Passive Mechanical Forces Control Cell-Shape Change during *Drosophila* Ventral Furrow Formation**Oleg Polyakov,<sup>1,\*</sup> Bing He,<sup>2</sup> Michael Swan,<sup>2</sup> Joshua W. Shaevitz,<sup>1</sup> Matthias Kaschube,<sup>4</sup> and Eric Wieschaus<sup>2,3</sup><sup>1</sup>Department of Physics, Princeton University, <sup>2</sup>Department of Molecular Biology, and <sup>3</sup>Howard Hughes Medical Institute, Princeton University, Princeton, New Jersey; and <sup>4</sup>Frankfurt Institute for Advanced Studies, Faculty of Computer Science and Mathematics, Goethe University, Frankfurt am Main, Germany

**ABSTRACT** During *Drosophila* gastrulation, the ventral mesodermal cells constrict their apices, undergo a series of coordinated cell-shape changes to form a ventral furrow (VF) and are subsequently internalized. Although it has been well documented that apical constriction is necessary for VF formation, the mechanism by which apical constriction transmits forces throughout the bulk tissue of the cell remains poorly understood. In this work, we develop a computational vertex model to investigate the role of the passive mechanical properties of the cellular blastoderm during gastrulation. We introduce to our knowledge novel data that confirm that the volume of apically constricting cells is conserved throughout the entire course of invagination. We show that maintenance of this constant volume is sufficient to generate invagination as a passive response to apical constriction when it is combined with region-specific elasticities in the membranes surrounding individual cells. We find that the specific sequence of cell-shape changes during VF formation is critically controlled by the stiffness of the lateral and basal membrane surfaces. In particular, our model demonstrates that a transition in basal rigidity is sufficient to drive VF formation along the same sequence of cell-shape change that we observed in the actual embryo, with no active force generation required other than apical constriction.

**INTRODUCTION**

During epithelial morphogenesis, internally generated forces drive an initial monolayer of epithelial cells to fold, transforming it into complex shapes with remarkable spatial and temporal precision (1–5). This process often involves a combination of localized, active force generation in the epithelial sheet and the passive mechanical responses to these forces. Because these mechanical responses arise from the intrinsic material properties of the tissue, maximizing their contribution to any morphogenetic process is advantageous in that it minimizes active energy requirements and simplifies the genetic patterning information necessary, resulting in a more physically robust system. Identification of such passive mechanisms also allows us to separate the genetic input from the preexisting mechanical conditions. This will not only help us to understand the underlying physical mechanism, but also allow us to pinpoint genetic steps that drive specific aspects of epithelial morphogenesis (6,7).

A system well suited for this study is the formation of the ventral furrow (VF) during *Drosophila* gastrulation. Before the onset of gastrulation, the *Drosophila* embryo undergoes cellularization to form the cellular blastoderm, which consists of ~5000 columnar cells arranged in an intact epithelial layer at the surface of the embryo. Immediately after the

completion of cellularization, a network of myosin II motors begins to accumulate in the apical domains of a  $14 \times 60$ -cell region on the ventral side of the embryo (6,7). Stochastic, pulsatile contractions of the actomyosin network generate contractile stress within the apical cortex of these cells, driving them through a series of coordinated cell-shape changes (8–11). During an initial slow phase, termed lengthening, the cells elongate along their apical-basal axis by a factor of ~1.7 while concomitantly reducing their apical areas. Next, the cells enter a fast phase, termed shortening, where they finish constricting their apices and rapidly shorten back to their original lengths, resulting in a final wedge shape as the tissue is internalized (12–15) (Fig. 1, A–C).

Although it has been well documented that apical constriction is necessary for VF formation, the mechanism through which apical constriction transmits force throughout the cell to drive cell-shape change remains poorly understood. In particular, it remains an open question whether the elongation and shortening phases observed in apically constricting cells are the result of a passive response of the tissue to the stress generated from apical myosin accumulation, or whether they are instead driven by an independent active process.

A number of computational models have been proposed to elucidate the cell-shape changes associated with gastrulation in various organisms (16,17), including *Drosophila* (18–27), sea urchin (28), and *Ascidian* (29). Similar models

---

Submitted September 12, 2013, and accepted for publication July 7, 2014.

\*Correspondence: [opolyako@princeton.edu](mailto:opolyako@princeton.edu)

Editor: Peter Hunter.

© 2014 by the Biophysical Society  
0006-3495/14/08/0998/13 \$2.00

---

<http://dx.doi.org/10.1016/j.bpj.2014.07.013>



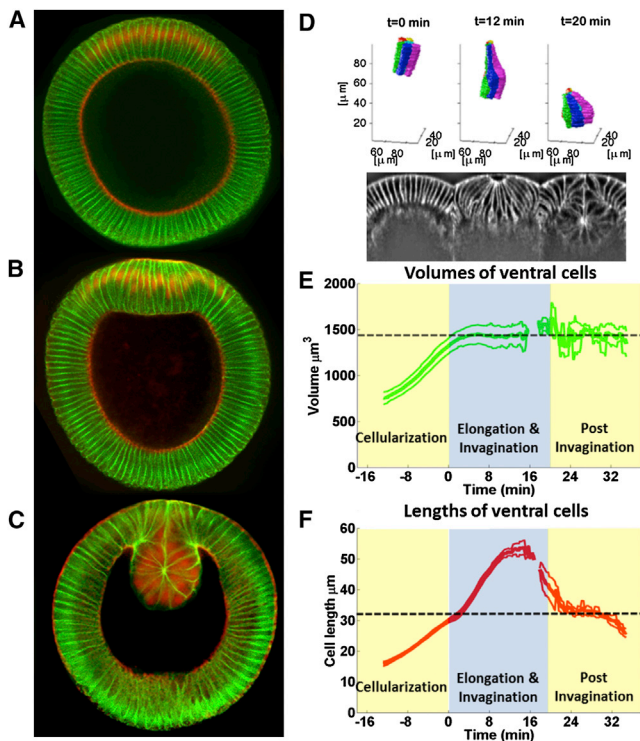


FIGURE 1 (A) Embryo cross section at the onset of gastrulation. Embryos are arranged ventral side up, showing the membrane (green) and Myosin (cortical) and Twist (nuclear) (red). (B) Lengthening phase of gastrulation. The ventralmost mesodermal cells undergo apical constriction and lengthen along the apical-basal axis. (C) Shortening phase of gastrulation. The elongated mesodermal cells shorten back to their original lengths, fully constrict their apices, and are invaginated into the interior. (D) Six reconstructed cells (upper row), shown with transverse cross sections (lower row), during the time course of gastrulation. From left to right, the time corresponds to the completion of cellularization ( $t = 0$  min), the end of lengthening during gastrulation ( $t = 12$  min), and the completion of invagination ( $t = 20$  min). (E) Volumes of individual reconstructed cells traced over the course of gastrulation. Data are represented as the mean  $\pm$  1 SD for  $n = 28$  cells. Time  $t = 0$  corresponds to the beginning of gastrulation. The  $\sim 20$  min time course of VF formation and invagination is shaded gray. (F) Lengths of ventral cells during VF formation (mean  $\pm$  1 SD,  $n = 28$  cells). The dashed line shows the average final cell lengths at the end of cellularization. To see this figure in color, go online.

have also been used to understand the mechanics of cell interactions in *Drosophila* wing disk formation (30,31). One of the first computational models of *Drosophila* gastrulation, by Odell et al., showed that constricting the apical surface leads to the buckling of the tissue and the formation of a furrow (18). In the pioneering works of Conte et al., Brodland et al., and Allena et al., invagination and furrow formation in elastic epithelial tissue was achieved by prescribing specific active cell deformations, such as apical constriction and apical-basal elongation of the mesodermal cells (21–23,25,26). The work of Pouille et al. approximated the cellular cytoplasm of the epithelium as a purely viscous fluid, which flows in response to an increase in apical-cortical tension (19). In this model, however, the formation

of a completely invaginated and closed furrow required an additional radial force that results from the curvature of the apical surface in the anterior-posterior direction. In the work of Brezavšček et al., it was shown that a combination of constant active tensions along the apical, lateral, and basal sides leads to furrow formation through stochastic buckling of the tissue along a random angular position (27). All of these models require active tensions or prescribed active cell deformations, in addition to apical constriction, to generate invagination. It is therefore unclear whether a purely passive model of tissue response can account for both furrow formation and the sequence of cell-shape changes.

To assess this possibility, we present here to our knowledge a novel model that investigates the passive mechanism minimally required to mediate furrow formation and cell-shape change in response to apical constriction. The main difference between our model and previous models is that we consider the spatially patterned stress due to apical constriction as the only active force input during the entire course of VF formation. In our model, there are no active forces present in the interior of the tissue. Instead, we propose that the forces present in the interior arise entirely from the tissue's passive mechanical response to apical constriction. We identify two main components of this passive response: the volume conservation of the incompressible cytoplasm and the cross-linked cytoskeletal meshwork lining the inner face of the plasma membrane (cell cortex). The incompressible cytoplasm allows apically generated contractile stress to be transmitted throughout the cell. To support our assertion, we present to our knowledge novel data confirming that cell volumes remain constant throughout VF formation. The cytoskeleton provides the cell with structural rigidity (32–34). We demonstrate that this passive mechanism, consisting of both cell-volume conservation and cortical elasticity, is sufficient to generate a closed and invaginated furrow in response to active apical constriction. The final morphology of the furrow and the sequence of cell-shape changes that result from this passive response are controlled by the amount of elasticity present on the apical, basal, and lateral surfaces of the tissue. As a result, our model is capable of reproducing the tissue morphologies seen at the end of the lengthening and shortening phases during in vivo VF formation. Intriguingly, we show that the cell-shape change pattern observed in the embryo, most notably the transition from the lengthening phase to the shortening phase, can be recapitulated in our model by a decaying stiffness of the basal surface. This mirrors the gradual disappearance of cytoskeletal components from the basal surface of the mesoderm cells during VF formation. Our model is therefore distinct from all previous models in that it is capable of achieving a closed and invaginated furrow along the same cell-shape change pattern observed in vivo without the requirement of any additional active forces in the tissue interior.

## MODEL

### Passive model equations and the initial equilibrium configuration

As the initial configuration for our model, we consider a 2-dimensional cross section of the fully cellularized embryo along the midpoint of its anterior-posterior axis (see Fig. 1, A–C). We use the onset of gastrulation as the starting point in our simulations. The initial configuration represents the cross section of a normal embryo, which corresponds to ~80 cells connected in a circle. These cells are bounded from the outside by the vitelline membrane and surround the inner yolk (Figs. 1 A and 2 A). We approximate each cell as a quadrilateral defined by its apical, basal, and lateral membrane surfaces (Fig. 2 B). Epithelial cells are connected through adhesive structures along their lateral membranes and thus our model cells share their lateral sides with their neighbors. In addition, we treat the vitelline membrane as a circular hard-core boundary condition that prevents the movement of the apical surface outside of its predefined radius (see section I of the Supporting Material).

Motivated by the results shown in Fig. 1 E, our model assumes that the volume of each individual quadrilateral cell remains constant throughout the simulation. We further presume that the cytoskeletal components lining the inside membrane surfaces of the cells provide these surfaces with springlike elastic properties. Because the *in vivo* distribution of myosin and actin varies along the apical, lateral, and basal surfaces, the spring constant of each surface is likely to be different. Our initial configuration is also our state of mechanical equilibrium. This means that the springlike cytoskeletal meshworks of the apical, lateral, and basal sides are relaxed and the total elastic potential energy stored in the initial configuration is zero.

To simulate the process of VF formation, we drive our model out of energy equilibrium through apically generated contractile forces. In contrast to previous models, we assume that the sequence of cell-shape change is controlled passively through the elasticity present on the cellular cortex. We ignore any elasticity of the cytoplasm (19,21,22), as well as the hydrodynamic flow attributed to the cytoplasm. Instead, the energy of our system is attributed to

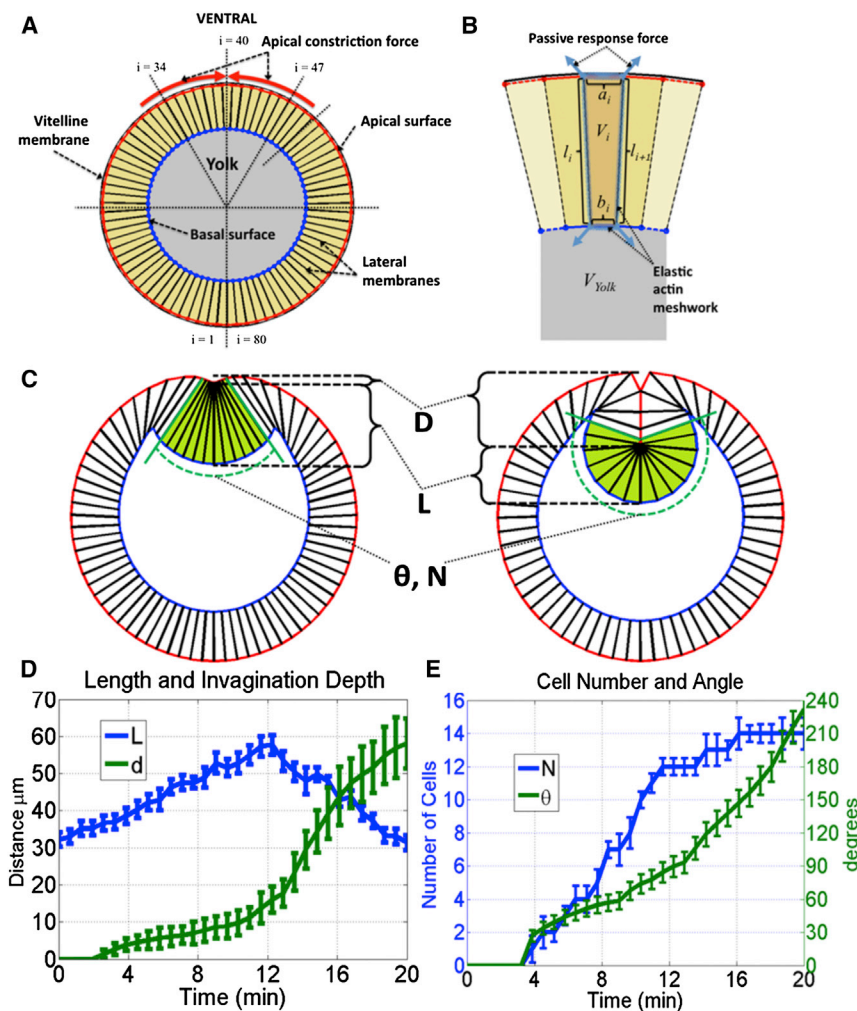


**FIGURE 2** (A) Vertex model of the cross section of the *Drosophila* embryo at the end of cellularization. The model is composed of 80 cells connected in a ring that surrounds the yolk. The cells in the ventral region are subjected to apical contractile stress. (B) Each cell is defined to be a unit of cytoplasmic volume  $V_i$  surrounded by the apical, lateral, and basal membrane surfaces. The rigidity of the membranes and the constant volume maintenance of  $V_i$  respond passively to the apical contractile stress to drive the cell-shape change. (C) Metrics used to characterize the VF. The invagination depth,  $d$ , and the average length of the ventral cells,  $L$ , are taken for the four ventralmost cells.  $N$  is the number of apically constricting ventral cells whose apical area is smaller than their basal area.  $\theta$  is the secant angle formed by the rosette arrangement of the  $N$  apically constricted cells. Values of  $\theta > 180^\circ$  generate furrows that are closed. (D and E) Measurements of  $L$ ,  $d$ ,  $N$ , and  $\theta$  made in live embryos over the course of gastrulation (mean  $\pm$  1 SD for four embryos). To see this figure in color, go online.

the active stress generation by apical constriction, the elastic response of the cellular cortex, and the incompressible cytoplasm and yolk.

The energy equation that approximates the mechanical properties of our system is given by the expression

$$E = \sum_i \varphi_i \mu_i a_i^2 + \sum_i [K_l (l_i - l_o)^2 + K_b (b_i - b_o)^2 + K_a (a_i - a_o)^2] + \sum_i C_{VOL}(V_i) + C_{YOLK}(V_{yolk}) \quad (1)$$

The first term in Eq. 1 represents myosin-mediated apical constriction and is the only active force in our model. This force is described in greater detail in section B below. The terms  $a_i$ ,  $b_i$ , and  $l_i$  are the apical, basal and lateral areas of cell  $i$ . The initial values of these variables are given by the constants  $a_o$ ,  $b_o$ , and  $l_o$  and are set to measurements made on embryos at the onset of gastrulation. The coefficients  $K_a$ ,  $K_b$ , and  $K_l$  are the relative spring constants that characterize the elastic resistance of the apical, basal, and lateral membranes to mechanical deformations. These coefficients are related to the rigidity of the actomyosin cytoskeletal meshwork that lines the membrane surfaces. The volume of each cell is  $V_i$  and the volume of the yolk is  $V_{yolk}$ .  $C_{VOL}$  and  $C_{YOLK}$  are constraint functions that ensure constant-volume maintenance of the individual cells and the yolk, respectively. The implementations of these constraints are discussed further in Appendix B.

For our model we assume homogeneity among all of the passive mechanical elements of the cell. Specifically, we assume that the constants  $K_a$ ,  $K_b$ , and  $K_l$  of Eq. 1, which characterize the elastic resistance to deformation of the apical, basal, and lateral surfaces, are the same for every cell at the onset of gastrulation. These are physical quantities and have units of N/m. Furthermore, we assume that the volume conservation mechanism,  $C_{VOL}$ , is also homogeneous among all of the cells. Together, the homogeneity of the mechanical properties of the cellular cortex, as well as the cytoplasm, defines the passive response mechanism of the cell and is the same for all cells.

### Active myosin-mediated apical constriction mechanism

In our model, the active force that provides the energy required for tissue morphogenesis is localized entirely on the apical surface of the epithelial layer (Fig. 2 A, red arrows). This force represents the stress generated due to the accumulation and subsequent contraction of apical myosin at the onset of gastrulation. In the gastrulating embryo, this active cytoskeleton undergoes dynamic pulsatile behavior and forms a global contractile network that extends across many cells through the connections of the adherens junctions. In individual cells, myosin pulses have been shown to correlate with decreases in apical area (8). When

averaged across the mesoderm, increased myosin led to a monotonically continuous reduction in apical area (8). When the VF is invaginated into the interior, the apical areas of the ventralmost cells are reduced to zero.

In our model, this active myosin-mediated apical constriction is represented by the term  $\varphi_i \mu_i a_i^2$  (Eq. 1). The apical force profile reflects the in vivo expression domains of the mesoderm specification genes *twist* and *snail*. *twist* activates the expression of a secreted protein, *folded gastrulation (fog)*, which in turn initiates the localization of apical myosin at the onset of gastrulation (13,15). Both *twist* and *fog* have a Gaussian distribution that is centered on the ventral midline, with the distribution of *fog* having a more narrow width than *twist*. We set the term  $\mu_i$  of our apical force profile to represent the spatial distribution of *fog*, which is modeled to be Gaussian-distributed around the ventral midline (Eq. 2a). Therefore, the term  $\mu_i$  represents the *fog*-mediated accumulation of apical myosin, which in turn is related to the physical stress that is applied to the apical surface. Meanwhile, the expression of *snail* is a step function that is symmetric and centered around the ventral midline. *snail* governs the expression of the *fog* receptor, *mist*, meaning that cells outside of the *snail* domain are not competent to respond to *fog*, and as a result, these cells do not accumulate myosin and produce no contractile force (7,14,35). We implement the effect of *snail* through the term  $\varphi_i$ , which is equal to 1 for cells within the *snail* domain and 0 otherwise (Eq. 2b). When multiplied together with  $\mu_i$ , the tail ends of the Gaussian distribution, which lie outside of the *snail* domain, are effectively truncated to zero. The term  $\varphi_i \mu_i$  therefore represents the spatial distribution of apical myosin, modeled on the in vivo activities of both *fog* (*twist*) and *mist* (*snail*). The width of the Gaussian distribution of  $\mu_i$  that we utilized for the results presented in the simulation was  $\sigma = 3.5$  cells. We chose  $\varphi_i$  such that the apical strength,  $\mu_i$ , is set to zero at  $2.5\sigma \approx 9$  cells away from the ventral midline, mimicking the roughly 18-cell-wide *snail* domain observed in vivo.

$$\mu_i = \mu_o e^{-\frac{(i-i_{mid})^2}{2\sigma^2}} \quad (2a)$$

$$\varphi_i = \begin{cases} 1 & |i - i_{mid}| \leq 2.5\sigma \\ 0 & \text{otherwise} \end{cases} \quad (2b)$$

The pulsatile contractility observed in vivo means that levels of myosin and the resulting reduction in apical cell area both fluctuate considerably over the course of gastrulation (8). We consider only the smooth reduction of apical area that represents the average effect of myosin in the cell. Furthermore, we assume that the magnitude of the total constriction force is proportional to the size of the apical area, which we believe to be a realistic assumption, as the area becomes very small. Therefore, the energy term that we utilize for apical constriction is a quadratic function of the apical area.

### Free parameters of the model and the classification of the final state

There are four free parameters that control the final outcome of our model. We rescale the main energy equation for our system (Eq. 1) by normalizing the coefficients of rigidity along the perimeter of the cells with respect to the maximum of the apical constriction strength,  $\mu_o$ . The resulting rescaled energy equation becomes

$$E = \sum_i \varphi_i e^{-\frac{(i-i_{mid})^2}{2\sigma^2}} a_i^2 + \sum_i [\alpha(l_i - l_o)^2 + \beta(b_i - b_o)^2 + \gamma(a_i - a_o)^2] + \sum_i C'_{VOL}(V_i) + C'_{YOLK}(V_{yolk}). \quad (3)$$

Here, the dimensionless normalized parameters  $\alpha = K_l/\mu_o$ ,  $\beta = K_b/\mu_o$ ,  $\gamma = K_d/\mu_o$ , and width  $\sigma$  become the set of free parameters that determine the final outcome of our model. These parameters characterize the rigidities of the lateral, basal, and apical surfaces and the width of the apical constriction domain. We begin all of our simulations in the initial configuration (Fig. 2 A) for constant values of  $\{\alpha, \beta, \gamma, \sigma\}$  and look for the energy minimum of Eq. 3 by iteratively updating the positions of the vertices along the direction of their gradient until a state of mechanical equilibrium is reached. This state equivalently corresponds to a minimum of the energy equation (Eq. 3).

### Quantitative measurements in wild-type embryos

To assess the validity of the assumptions of our model, as well as to quantitatively compare the results of our model with live measurements of wild-type embryos, we generated three distinct data sets. First, we made to our knowledge novel measurements of cell volumes and lengths during the entire course of VF formation. These measurements were made using EDGE software, which uses microscope optical sections to reconstruct the 3-dimensional shape of ventral cells during VF formation in living embryos (36). The image stacks for these experiments were acquired at 12- or 18-s intervals using a two-photon microscope. Measurements were made on cellularizing and gastrulating embryos whose cell membranes were marked with E-cadherin-GFP.

Second, to quantitatively compare the cross-sectional morphology of our model to those achieved by wild-type cells, we imaged E-cadherin-GFP-labeled embryos and reconstructed their two-dimensional cross sections throughout VF formation. We quantitatively compared the cross sections of real embryos to those of our model by defining a set of measures that uniquely describe the furrow shape during gastrulation. We make use of two metrics:  $d$ , defined as the average invagination depth of the apical surface with respect to the vitelline membrane; and  $L$ , defined as the

average apical-basal length of the two ventralmost cells. As an additional metric, we take advantage of the observation that VF cells undergoing apical constriction will naturally try to arrange into a rosette structure by expanding their basal surfaces and inverting their curvature. To characterize the resulting shape of this region, we introduce  $N$ , the number of cells whose apical surfaces are smaller than their basal surfaces, as well as the rosette angle,  $\theta$ , which measures the secant angle enclosed by those cells (Fig. 2 C). For those values of  $\theta > 180^\circ$ , the two sides of the apically constricting region touch, resulting in a rosette of cells that forms a closed furrow. Using these metrics, we confirmed that wild-type gastrulation proceeds in two distinct stages (Fig. 2, D and E). During the initial lengthening stage (0–12 min), the apical surface of the ventralmost cells constricts to  $\sim 30\%$  as they slowly elongate to a maximum length of  $L_{max} \approx 1.7l_o$ , where  $l_o = 32 \mu\text{m}$  is the initial length of the tissue. Concomitantly, the apical surface invaginates slightly to a value of  $d \approx 0.4l_o$ . At the end of the lengthening phase, the open and shallow furrow is composed of  $N \approx 12$  cells with a rosette angle of  $\theta \approx 88^\circ$ . Next, the embryo enters the shortening stage (12–20 min), where the ventralmost cells rapidly shorten to their original lengths,  $L \approx l_o$ . At the same time, these cells continue to reduce their apical areas to zero while significantly expanding their bases. This invaginates the apical surface deep into the embryo, to a depth of  $d \approx 1.8 \cdot l_o$ . Basal surface expansion produces a final rosette angle of  $\theta \approx 210^\circ$  made up of  $N = 14$  cells, thereby generating a closed and invaginated furrow. These measurements provide the basis for a direct comparison of VF formation between the living embryos and our simulation.

Finally, we quantified the dynamics of myosin on the basal surface of the invaginating mesoderm as a potential indicator of the rigidity of the basal surface. To obtain these measurements, we immunostained fixed embryos and sectioned them by hand. Myosin was visualized using an antibody against *zipper*, the myosin heavy chain. Antibodies against *twist* and *neurotactin* were used to visualize mesodermal nuclei and cell membranes, respectively. Confocal images were acquired at the transverse cross section plane of the embryo with a Z-step of  $0.5 \mu\text{m}$ . Using custom designed software, described in greater detail in section J of the [Supporting Material](#), we measured myosin levels along the basal surface of the mesoderm and the ectoderm over the course of gastrulation. These measurements revealed that myosin levels decrease significantly in both the ectoderm and mesoderm during the shortening phase of VF formation. Strikingly, basal myosin is depleted to a far greater extent in the mesoderm than in the ectoderm, resulting in almost total depletion by the end of the shortening phase. These measurements identified a previously unknown mechanism that could be responsible for apical-basal tissue shortening during VF formation. To investigate this possibility using our model, we mimicked the in vivo

decrease of basal myosin by decreasing the rigidity of the basal surface.

## RESULTS

### Validation of constant-volume maintenance

Because the contractile myosin II network is present only on the apical surface of the mesodermal cells, contractile stress is constrained to the plane of the apical surface. To be capable of driving the tissue through an out-of-plane deformation, this stress must first be transmitted throughout the cell along the radial direction. We propose that contractile stress transmission is possible because cells maintain a constant volume while undergoing morphogenesis. Constant-volume maintenance approximates the forces generated by the viscous displacement of an incompressible cellular cytoplasm, providing a passive mechanism by which apically generated stress is instantaneously transmitted throughout the cell.

To confirm that cell volume is indeed conserved throughout VF formation, we reconstructed cell shapes of the ventralmost cells from cellularization, through VF formation, to the movements initiated by germ-band extension (Fig. 1 D). In the period that precedes gastrulation, cell volumes increase as the cells undergo cellularization. Over the

course of gastrulation, however, mesoderm cell volumes remain constant despite large fluctuations in their length (Fig. 1, E and F, gray region). These experimental findings justify the use of volume conservation as a passive mechanism to drive cell-shape changes in response to apical stress. We refer the reader to section E of the [Supporting Material](#) for possible mechanisms through which cells maintain their volume during VF formation.

### The combination of apical constriction, constant-volume maintenance, and an elastic cortex is sufficient to generate a closed and invaginated furrow

To investigate the effect of local cortical elasticity on invagination, we held apical constriction constant and simulated a final model phenotype for a range of lateral and basal rigidities (Fig. 3 A). For these simulations, the size of the constricting apical domain was held constant at  $\sigma = 3.5$  cells. For a discussion of the apical rigidity parameter,  $\gamma$ , we direct the reader to section G of the [Supporting Material](#). The furrow phenotypes that result from this simulation reveal several features of the impact of local rigidity on VF formation.

First, a minimum amount of lateral rigidity is required for the invagination of the apical surface. As lateral rigidity,  $\alpha$ ,

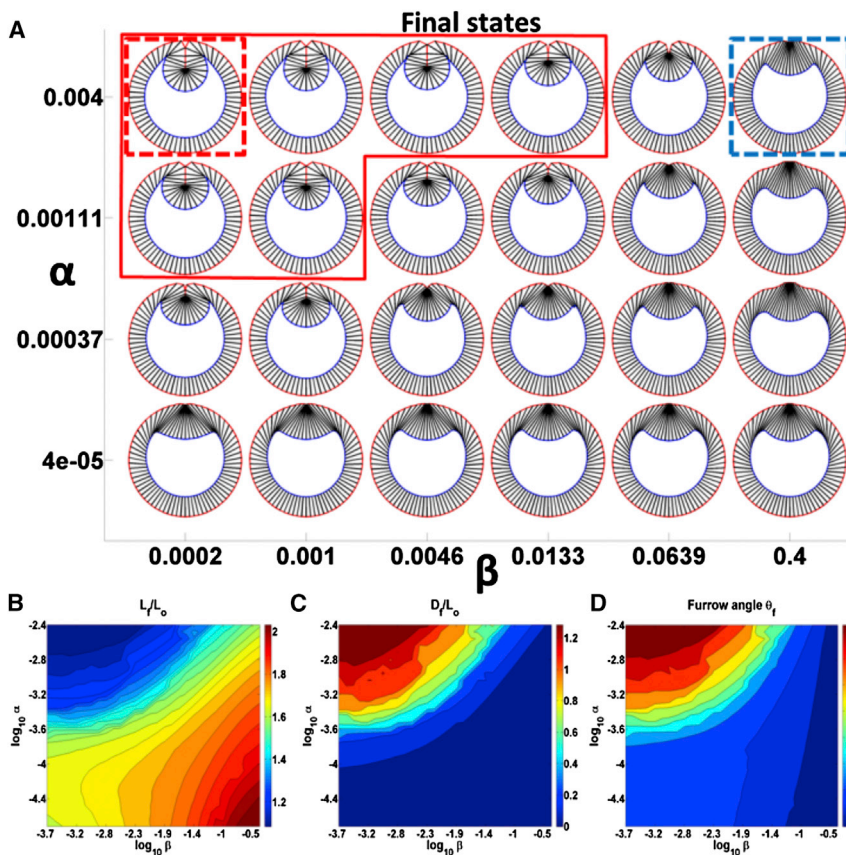


FIGURE 3 (A) Energy-minimum configurations for the two free parameters  $\alpha$  and  $\beta$ . The solid red line indicates the set of those states that have a final rosette  $\theta_f$  angle  $>180^\circ$  and evolve to form a closed and invaginated furrow. The model configurations that best approximate the embryo at the end of the lengthening and shortening phases are given by the dashed blue and red boxes, respectively. The values of the other two free parameters remain constant at  $\gamma = 6.0 \times 10^{-3}$  and  $\sigma = 3.5$  cells. (B–D) Furrow measurements for the final state. Final cell length,  $L_f$ , final invagination depth,  $d_f$ , and final rosette angle,  $\theta_f$ , versus  $\alpha$  and  $\beta$ . To see this figure in color, go online.

approaches 0, the tissue does not invaginate for any given value of basal rigidity,  $\beta$  (Fig. 3 A, bottom row). The passive mechanism of volume conservation and lateral rigidity through which apical constriction can produce the out-of-plane deformation necessary for invagination can be described as follows. As the apex of an individual cell constricts, isotropic pressure is generated due to the constant-volume constraint. This pressure pushes against the cell surface as it tries to restore the volume. Because the apical and lateral sides of the cell are bound by the vitelline membrane and the neighboring cells, respectively, the pressure pushes the basal side of the cell toward the yolk and begins to stretch the lateral surface. Due to the rigidity of the lateral surface, a resulting springlike restoring stress due to the rigidity of the lateral surface subsequently pulls the apical surface inward and causes it to invaginate.

Second, the critical parameter that controls the final furrow shape is given by the ratio of the lateral rigidity to the basal rigidity,  $\alpha/\beta$ . Within the set of values where  $\alpha/\beta > \sim 1.5$ , the system evolves to a final energy-minimum configuration that resembles the closed and invaginated furrow observed in vivo. In this configuration, the furrow has a final rosette angle of  $\theta_f \geq 180^\circ$ , with an average invagination depth of  $d_f = 1.35l_o$  and a final cell length close to the initial equilibrium value of  $L_f = 1.08l_o$  (Fig. 3 A, solid red outline). In this regime, the rigidity of the lateral surface is sufficiently higher than the rigidity of the basal surface to allow apically constricting cells to maintain constant volume exclusively through the expansion of their basal surfaces, which allows the tissue to acquire the fully invaginated configuration (Fig. 3 A, solid red outline).

In regimes where  $\alpha/\beta < 1.5$ , the final energy-minimum configurations of our model have furrows with smaller invagination depths,  $d_f$ , smaller rosette angles,  $\theta_f$ , and larger final cell lengths,  $L_f$  (Fig. 3, B–D). These configurations result from either a decrease of the passive lateral restoring force or an increase in the rigidity of the basal surface. Specifically, for constant values of  $\beta$ , decreasing the lateral rigidity,  $\alpha$ , allows the apically constricting cells to elongate their lateral membranes, becoming longer and thinner. The lack of the lateral restoring force results in furrows that have smaller rosette angles,  $\theta_f$ , and invaginate less into the interior. As the value  $\alpha$  approaches 0, apically constricting cells change their shape exclusively through apical-basal elongation and form furrows with invagination depth  $d_f = 0$  (Fig. 3 A, lower). In a similar way, for constant values of  $\alpha$ , increasing the basal rigidity,  $\beta$ , achieves final model configurations that do not form closed furrows and do not invaginate. In this case, a high value of  $\beta$  restricts the expansion of the basal surface, thus forcing the apically constricting cells to maintain a constant volume by elongating their lateral membranes. However, in this scenario,  $\alpha$  is not small, so the lateral membranes store elastic energy as they stretch ( $L_f = 1.65l_o$  for Fig. 3 A, upper right) and

thus are able to cause a slight invagination of the apical surface to  $d_f = 0.2l_o$ .

### Reduction of basal rigidity induces lateral shortening and forms a closed and invaginated furrow

In *Drosophila* embryos, the process of VF formation is characterized by two distinct phases of cell-shape change. First, ventral cells constrict apically and elongate along the apical-basal direction. Subsequently, these cells shorten back to their original lengths as the furrow invaginates. By varying cortical rigidities, we found that our model is capable of producing final phenotypes that mimic the shape of cells observed in vivo at the end of the lengthening phase (Fig. 1 B), as well as the closed and invaginated furrow seen at the end of the shortening phase (Fig. 1 C). The final energy-minimum configuration that best approximates an embryo at the end of the lengthening phase is given by the parameters  $\alpha = 4 \times 10^{-3}$ ,  $\beta = 0.4$  (Fig. 3 A, dashed blue box). As in normal embryos (Fig. 2, D and E), this state is composed of long, thin cells that reach a maximum elongation of  $L_f = 1.65l_o$  without much invagination of the apical surface ( $d_f = 0.2l_o$ ). The basal surface undergoes almost no expansion and has a final rosette angle of about  $\theta_f \approx 80^\circ$ . The postinvagination, with the embryo closed and the furrow invaginated, is best approximated by values of  $\alpha = 4 \times 10^{-3}$ ,  $\beta = 2 \times 10^{-4}$  (Fig. 3 A, dashed red box). The furrow cells are wedge-shaped, with the apical ends constricted and the basal ends expanded. The final length is close to  $l_o$  and the furrow depth ( $d_f \approx 1.35l_o$ ), angle ( $\theta_f \approx 200^\circ$ ), and cell number ( $N_f = 14$ ) are in good agreement with in vivo measurements.

By varying the ratio of basal to lateral rigidity, our model is capable of producing final configurations that closely resemble embryos at the end of the lengthening or shortening phases of VF formation. Since this ratio governs the final shape of the furrow, we hypothesized that modulation of this ratio could explain why invagination proceeds through these two distinct phases. We tested this prediction by further evolving the elongated final-state configuration (Fig. 3 A, dashed blue box) for decreasing values of  $\beta$ . In fact, over a range of  $\beta = (2 \times 10^{-4}, 0.4)$  ( $\alpha = 4 \times 10^{-3}$ ,  $\gamma = 6.0 \times 10^{-3}$ ,  $\sigma = 3.5$  cells), we can systematically control the invagination depth,  $d_f$ , the furrow angle,  $\theta_f$ , and the length of the furrow,  $L_f$ , between the elongated state and the state that forms a closed and invaginated furrow. This effectively allows the model system to reach energy-minimum configurations that correspond to the time course of furrow formation observed in living embryos, in particular the latter half that corresponds to shortening and the subsequent invagination of the tissue.

Fig. 4 A shows the final energy configurations along the time course of furrow formation for an initial state characterized by the parameter set  $\alpha = 4 \times 10^{-3}$ ,  $\beta = 0.4$ ,

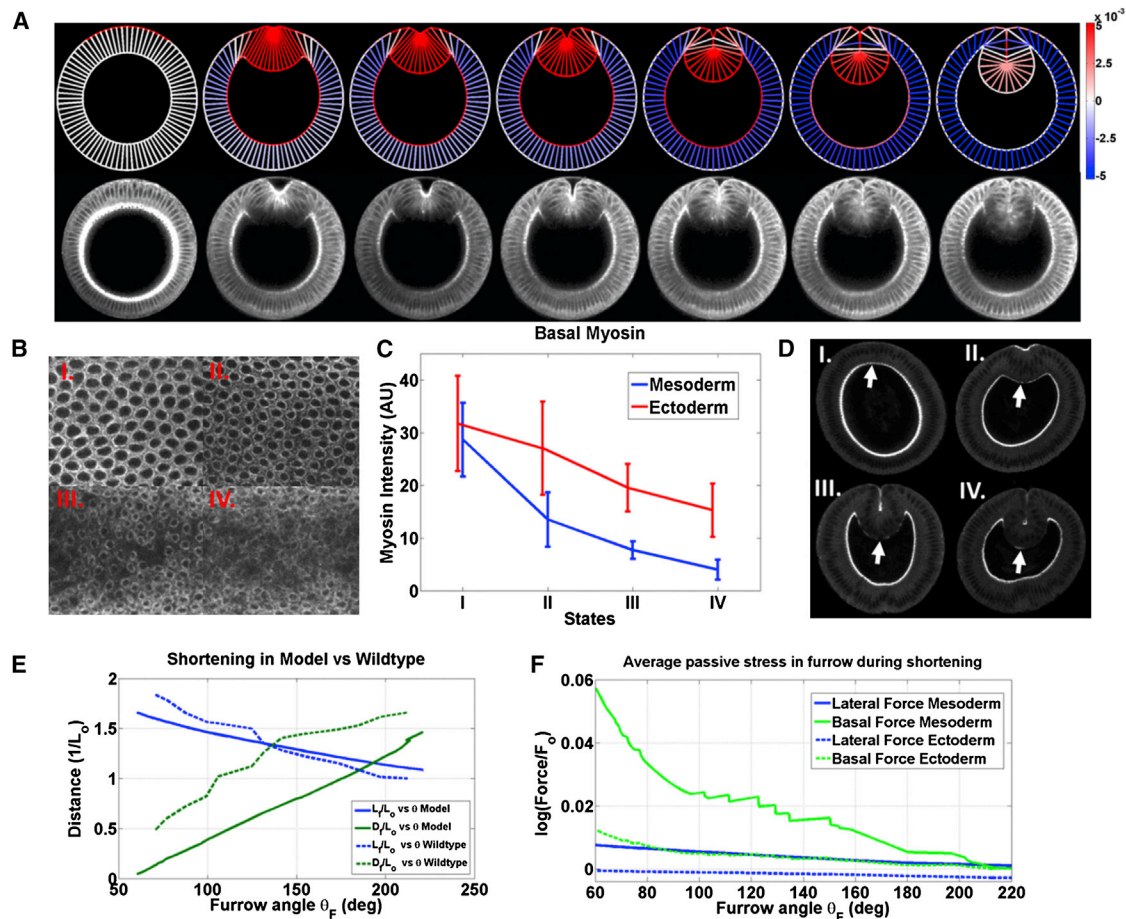


FIGURE 4 (A) Cell shortening and furrow invagination by decreasing  $\beta$ . The first frame is the starting configuration. The second frame is the energy-minimum configuration defined by  $\alpha = 4 \times 10^{-3}$ ,  $\beta = 0.4$ ,  $\gamma = 6 \times 10^{-3}$ ,  $\sigma = 3.5$ . The following frames are energy-minimum states as  $\beta$  is slowly reduced from 0.4 to 0. The color bar shows passive forces normalized to  $\mu_o$ . Red corresponds to stretching forces and blue to compression forces. (B) Two-photon images of basal myosin at different states of VF formation. (C) Decrease of myosin intensity on the basal surface in the mesoderm and the ectoderm ( $N = 5$  embryos). (D) Cross section showing myosin staining at different states of VF formation. Arrows indicate basal myosin in the mesoderm. (E) Invagination depth and furrow length as a function of furrow angle between the model and the wild-type. (F) Average basal and lateral passive forces in the mesoderm and ectoderm during shortening induced by the decay of  $\beta = 0.4 \rightarrow 0$ . Upon the decrease of basal rigidity, the mesodermal cells utilize the elastic energy stores in their lateral membranes to invaginate the apical surface. To see this figure in color, go online.

$\gamma = 6.0 \times 10^{-3}$ ,  $\sigma = 3.5$  cells as the basal rigidity,  $\beta$ , is slowly reduced to zero. During this transition, the model reproduces many key features observed in living embryos during shortening and invagination. In particular, the ventralmost cells shorten from  $L_f = 1.65l_o$  to  $L_f = 1.08l_o$  as the furrow closes. At the same time, the tissue invaginates to a depth of  $d_f = 1.35l_o$  as the furrow rosette angle expands from  $\theta_f = 80^\circ$  to  $\theta_f = 200^\circ$  (see Fig. 4 E for comparison to measurements made in living embryos). Furthermore, in both the model and the embryo, the final configuration of the furrow is composed of  $N_f = 14$  cells. In the simulation shown in Fig. 4, the decrease of basal rigidity,  $\beta$ , is applied equally to the basal surface of all cells. However, only in the mesoderm is it critical that  $\beta$  is completely reduced to zero. A partial reduction of  $\beta$  in the ectoderm has no effect on the lengthening-to-shortening transition (data not shown).

These results suggest that in the gastrulating embryo, a reduction of basal rigidity could be the primary trigger that causes the transition from cell lengthening to cell shortening and tissue invagination. At  $\beta = 0.4$ , high basal rigidity would restrict the expansion of the basal surface, preventing invagination and forcing the apically constricting cells to instead elongate along the apical-basal direction. This results in an energy-minimum configuration corresponding to the end of the lengthening phase. In this elongated state, passive mechanical potential energy is stored in the stretched lateral membranes (Fig. 4 A, see color bar for force magnitude). Upon the transition from  $\beta = 0.4$  to  $\beta = 0$ , basal surface expansion allows the lateral membranes to shorten to their equilibrium value,  $l_o$ . In doing so, lateral membranes utilize their stored potential energy to generate a restoring force along their apical-basal axes that drives the invagination of the apical surface.



The close concordance of our model with live embryos led us to investigate whether some biological process could cause a reduction in basal rigidity during gastrulation. At the beginning of *Drosophila* cellularization, myosin accumulates at the leading edge of invaginating membranes. This hexagonal meshwork of basal myosin remains associated with the invagination front for the duration of cellularization (Fig. 4 B, I). Near the end of cellularization, basal myosin organizes into individual contractile rings, which constrict to close off the cells basally, compartmentalizing the epithelium (Fig. 4 B, II) (33). Myosin is also present at uniform, lower levels between contractile rings (Fig. 4, B and C). Close to the end of cellularization, myosin begins to disappear from the basal side of mesodermal cells. This trend continues over the course of gastrulation. We quantified this decrease in basal myosin over time by immunostaining embryos for *zipper*, the *Drosophila* myosin heavy chain. By the end of VF formation, the average amount of basal myosin intensity in the mesoderm drops to nearly zero, a 10-fold decrease, whereas basal myosin intensity in the ectoderm decreases by only a factor of 2 (Fig. 4, C and D). This dramatic decrease of basal myosin in mesodermal cells occurs simultaneously with the expansion of their basal surfaces during VF formation. This suggests that the presence of basal myosin during the lengthening phase may provide the basal cortex with the additional rigidity necessary to passively resist the deformation of the basal surface. The decay of basal myosin could signify a reduction of this basal rigidity, permitting the basal expansion characteristic of the shortening phase.

Overall, our model demonstrates that by decreasing basal rigidity,  $\beta$ , we are able to form a closed and invaginated furrow that follows the same patterns of cell-shape changes that occur in the embryo (Fig. 4, A and E). It is important to note that the decay of  $\beta$  does not require generation of any additional active force in the tissue interior and therefore represents a purely passive mechanism that mediates cell lengthening, shortening, and tissue invagination in response to apically generated contractile stress. In addition, we identify the reduction of basal myosin in the mesoderm as a potential mediator of the transition between the lengthening and shortening phases of VF formation.

### Apical stress distribution determines the final furrow phenotype

In our model, active contractile stress, distributed along the apical surface, provides all of the input energy to drive the system from the initial configuration to the final state. The shape of this distribution uniquely determines not only the region of apically constricting cells but also the shape of those cells that border the constricting region. The final shape of the resulting invagination is thus a product of cell-shape changes both in the mesoderm and in the bordering ectoderm. We systematically modeled the effects

of different apical contractile stress distributions and found that a smooth gradient of stress centered on the ventral midline is necessary to generate a closed and invaginated furrow. This suggests that nonuniform constriction of the apical surface is required for invagination. In contrast, distributions that uniformly constricted the apices of a region of cells caused excessive stretching of the neighboring cells, preventing the tissue from invaginating (see section D of the [Supporting Material](#)). We speculate that a smooth gradient of apical contractile stress permits invagination because cells at the mesoderm/ectoderm boundary can balance their individual apical constriction with the pull resulting from the apical constriction of their neighbors. In accordance with this finding, both the intensity of apical myosin and apical tension measured by video force microscopy suggest that myosin is distributed in a smooth gradient across the mesoderm, with the peak centered on the ventral midline (24) (see section A of the [Supporting Material](#)). Although previous models of VF formation usually prescribe uniform tension across the mesoderm, we propose for the first time to our knowledge that in the embryo, genetic patterning information may underlie this tuned gradient of apical constriction.

In our model, we drive invagination and furrow formation by a Gaussian-distributed apical strength parameter,  $\mu_i$ , together with a steplike distributed parameter,  $\phi_i$ , that truncates the tail ends of the distribution of  $\mu_i$ . We found that the final shape of the furrow critically depends on the width,  $\sigma$ , which characterizes the width of the apical stress distribution (Eqs. 2a and 2b). Fig. 5 A shows the final state for the parameters  $\{\alpha = 4 \times 10^{-3}, \beta = 0.2 \times 10^{-4}, \gamma = 6.0 \times 10^{-3}\}$  for different values of  $\sigma$ . The effect of increasing  $\sigma$  on the final shape of the furrow is nonmonotonic. For values of  $\sigma < 7.4$ , the final number of furrow cells,  $N_f$ , increases with  $\sigma$ , because  $\sigma$  effectively determines the size of the apically constricting domain. Higher values of  $\sigma$  also result in larger invagination depths,  $d_f$ , since larger furrows push deeper into the interior. In contrast, for values of  $\sigma > 7.4$  the number of furrow cells,  $N_f$ , abruptly decreases as  $\sigma$  increases. In this regime, the process of furrow formation is disrupted and the furrow remains open. Expansion of the domain of apical constriction increases the amount of basal expansion necessary to accommodate all of the apically constricting cells in a larger invaginated furrow. For values of  $\sigma > 7.4$ , the geometric configuration of the model precludes the required amount of basal expansion, preventing invagination. These results suggest that the domain of apical constriction is evolutionarily tuned to be large enough to allow the formation of a furrow but not so large that furrow formation is prevented by the geometric constraints of the embryo. On the other hand, the observation that furrow formation can be achieved within a relatively broad range of values of  $\sigma$  suggests that such a system can tolerate some degree of variation in the input of active forces.

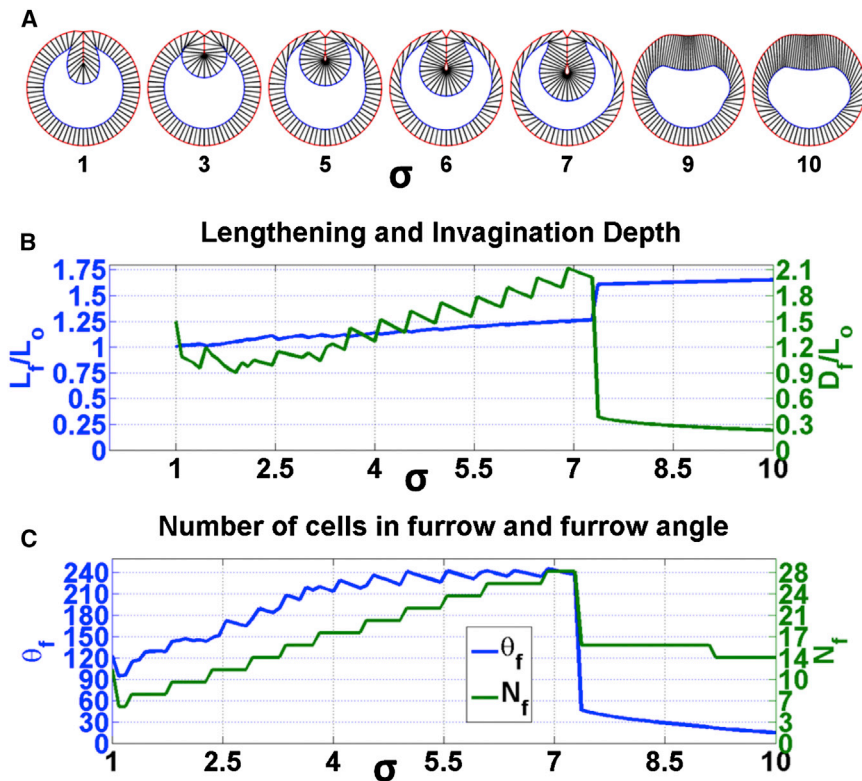


FIGURE 5 (A) Energy-minimum configurations for different widths of the apical constriction distribution defined by the width parameter  $\sigma$ . (B) Lengthening and invagination depth for different  $\sigma$ . The size of the apical constriction distribution is capable of controlling the extent of tissue invagination but is incapable of significantly changing the extent of cell lengthening. (C)  $\sigma$  determines the size of the apically constricting region by increasing the number of apically constricted cells in the furrow,  $N_f$ . For  $\sigma > 7.4$ , excessive apical constriction disrupts invagination and prevents the furrow from closing. To see this figure in color, go online.

Interestingly, unlike  $\alpha$ , the parameter  $\sigma$  is unable to significantly change the amount of cell lengthening during the process of invagination (Fig. 5 B,  $\sigma < 7.4$ ). States at different  $\sigma$  will evolve to different final furrow configurations while maintaining the lengthening of the lateral surfaces within the range determined by  $\alpha$ . Those states at higher values of  $\alpha$ , which restrict the range of cell elongation, are more significantly affected by the width of the apical constriction profile, due to the increased constraint of maintaining constant lateral lengths. Thus, although decreasing  $\alpha$  generates furrows by increasing the number of cells and lengthening them, increasing  $\sigma$  generates furrows that have more cells but do not elongate.

## DISCUSSION

Our working computer vertex model demonstrates that passive volume maintenance can function as the primary mechanism that governs the transmission of apically generated forces throughout the whole length of the cell. Within the given parameter ranges of  $\{\alpha, \beta, \gamma, \sigma\}$  our model proposes a mechanism that is capable of producing tissue invagination and formation of a closed VF when driven by spatially patterned apical constriction. Both the final in silico VF shape and the final shape of individual cells bear strong resemblance to those observed in living embryos. In particular, the model furrow is composed of 14 cells, connected in a rosette that invaginates into the interior and is closed by the pulling together of the opposite ends of the mesodermal

apical surface. In addition, our model is able to reproduce the lengthening and shortening dynamics that characterize the cell-shape change process of VF formation in vivo. Furthermore, the cells that form the final closed and invaginated furrow are wedge-shaped. The ectodermal ventral dorsal thinning observed in the wild-type is also present in the model.

The main assumption underlying our model is the presence of an elastic membrane cortex. Currently, there are no in vivo rheological measurements to elucidate the mechanical properties of membranes in *Drosophila* embryos. Thus, it is not known whether membranes in the embryo are elastic or whether that elasticity exists on a timescale relevant for VF formation. We assume the source of elasticity to be the cross-linked and entangled actin meshwork lining the interior cortex of the cell membrane, since the elastic properties of such cortical networks have been established in other systems (37,38). In particular, previous experiments measuring the elastic response of axons in isolated neurons have demonstrated that axons are able to rapidly revert to their original length after being stretched for tens of minutes, suggesting that the cell cortex could have an elastic response on the timescale of VF formation (39). The results of our model show that if such a passive mechanism does exist, it could account for tissue invagination, furrow formation, and also the lengthening/shortening dynamics of cell-shape change.

In contrast to previous models of VF formation, our model is unique in several important aspects. First, in our

model the only prescribed active force is that of apical constriction. With the absence of any additional forces in the tissue interior, our model is intended to test whether VF formation can be driven by a purely passive response of the tissue to apical constriction. This approach is fundamentally different from those of models that require additional active forces in the tissue interior to generate an invagination that resembles the embryo. Some previous attempts to model invagination have used cell-shape changes as inputs to drive tissue deformation (20,23). In our model, on the other hand, cell-shape changes are the result of the mechanical response of each cell to active apical constriction. Second, distinct from the viscous or viscoelastic models, our model does not account for the viscosity of the tissue and therefore does not try to reproduce the exact dynamics of tissue deformation. Third, our model does not have a time term in the governing equations. Thus, once the system is driven out of equilibrium, it transits to another equilibrium state instantaneously. Finally, although the goal of our model is to investigate principles that can lead to furrow formation with a minimal input of prescribed active forces, we have put a particular emphasis on precisely reproducing the shape of the actual VF and recapitulating the characteristic sequence of cell-shape changes seen in vivo.

Our simulation confirms the earlier notion by Odell et al. that apical constriction alone is sufficient to drive VF invagination and that no additional active forces are absolutely required (18). We further extend this notion by showing that such a mechanism not only can drive the formation of a closed furrow but can do so through the same path of cell-shape changes observed in vivo. Whereas all previous models that have sought to reproduce the actual in vivo cell morphologies in the context of complete mesoderm internalization are rather complex and necessitate additional forces other than apical constriction, our model, for the first time to our knowledge, achieved this goal through a passive mechanism that minimizes the requirement of prescribed active force input. Such a mechanism may be beneficial in development, because it reduces the requirement of complex genetic pre patterning and thus increases the robustness of morphogenesis.

Our model identifies a passive springlike restoring force, resulting from the structural rigidity of the lateral membranes as the primary passive force that drives the invagination of the apical surface. When  $K_l < \mu_o(1 \times 10^{-4})$  ( $\alpha < 1 \times 10^{-4}$ ), no invagination occurs. In contrast, the tissue still invaginates when rigidity is absent on the apical or basal surfaces ( $\gamma = 0$  or  $\beta = 0$ ), which suggests that rigidity along the lateral surface, but not along the apical or basal surface, is absolutely required for tissue invagination. Interestingly, if we assume that the parameters remain constant during invagination, for our model to best approximate the final wild-type morphology  $\{\alpha = 4 \times 10^{-3}, \beta = 2 \times 10^{-4}, \gamma = 6.0 \times 10^{-3}\}$ , the lateral restoring force must be set strong

enough to almost entirely restrict any tissue elongation. This high lateral restoring force blocks the initial lateral elongation that is observed in vivo. Conversely, a weaker lateral restoring force will allow initial tissue elongation during apical constriction, but the final length will not be restored to  $l_o$ , preventing complete tissue invagination. These results suggest that for constant cellular membrane rigidities and constant active apical constriction, it is not possible for furrow formation to proceed along the pattern of cell-shape changes observed in vivo. However, distinct membrane rigidities generate furrows that resemble the end point of each phase of invagination observed in vivo. This suggests that the embryo may modulate membrane rigidities, which results in the two distinct phases of invagination.

By investigating the transition of the lengthened minimal energy configuration to the shortened, invaginated configuration, we showed that the systematic decay of basal rigidity,  $\beta$ , creates a furrow with the same lateral lengthening-to-shortening transition dynamics as seen in vivo. In this scenario, the model embryo transitions from an elongated state to an invagination along a series of energy equilibrium points that are defined by  $\beta$ . The initially strong basal rigidity arrests invagination in the elongated state, where the apically constricting cells are stretched laterally to a maximum amount of  $1.65l_o$ . The subsequent systematic decay of  $\beta$  provides the rate-limiting step in the transition to an invaginated state and allows the cells to return to their original length as they form the closed furrow.

Analysis of immunostained embryos revealed that the amount of basal myosin in the mesoderm decreases throughout the lengthening phase and disappears right before the onset of the shortening phase. We propose that this reduction of basal myosin in the embryo is analogous to the systematic decay of  $\beta$  that drives invagination in our model. Initially, the presence of strong basal myosin at the onset of gastrulation confers a high basal rigidity, which leads to lateral tissue elongation upon apical constriction. Over the course of gastrulation, the loss of basal myosin reduces basal rigidity, eventually triggering the rapid transition to an invaginated state. Since basal myosin decay is much more pronounced in the mesoderm than the ectoderm, the process could be developmentally regulated to precisely modulate the passive response of the mesoderm tissue to apically generated forces. In the future, it will be crucial to verify and measure the ability of the lateral membranes to store elastic energy. Furthermore, it will be interesting to determine how the embryo modulates the cortical cytoskeleton.

Our model provides important insight into the spatial distribution of the active constriction stress along the apical surface. When combined with passive cortical elasticity, this active apical stress is necessary and sufficient to invaginate the tissue and form a closed furrow. The shape of this distribution of apical constriction magnitudes uniquely

determines the shape of the resulting furrow. Since only certain distributions generate a closed furrow, this shape must be evolutionarily tuned to the geometry of the embryo. Outside of this tuned value, the geometry of the embryo precludes the packing of constant-volume-constrained cells into a furrow. Our model demonstrates that a trimmed Gaussian distribution of apical constriction recapitulates *in vivo* invagination with high fidelity. This distribution was chosen because it reflects the spatial distribution in the embryo of mesodermal patterning genes and their downstream targets, which are responsible for activating apical constriction (40,41). Myriad genetic and molecular tools exist in *Drosophila* to perturb embryonic patterning. Future work will focus on the manipulation of apical constriction to test the predictions of the model.

In summary, our model represents to our knowledge a novel and unique approach to understand the mechanical mechanism underlying *Drosophila* VF formation. By identifying the minimalistic passive, as well as active, mechanisms, our study sheds light on the mechanical properties of cellular structures that are critical for gastrulation. These insights broaden our knowledge, both biological and physical, of the interplay between genetics and mechanics in the process of tissue morphogenesis.

## APPENDIX A: CONSTANT VOLUME CONSTRAINT IMPLEMENTATION AND YOLK COMPRESSIBILITY

In our model, we implement the constant volume constraint for individual cells by assigning an energy term,  $C_{VOL}(V_i)$ , in the main energy equation (Eq. 1). This term penalizes deviations of the volume,  $V_i$ , from the initial value,  $V_o$ , for each cell  $i$ . For the volume conservation of individual cells, we utilize the equation

$$C_{VOL}(V_i) = K_V(V_i - V_o)^2. \quad (4)$$

Here, the value of the parameter  $K_V$  controls deviations of volume  $V_i$  from the initial volume,  $V_o$ , for each cell  $i$ . All of the simulations presented in this manuscript use the value  $K_V = 100$ , which restricts the maximum deviation of the volume to  $\sim 0.5\%$  of the initial value.

We likewise assume that the yolk resists compression. In addition, we implement an outward yolk pressure that reflects the high hydrostatic pressure that we observe in the embryo. This outward pressure pushes on the basal surface of the ectoderm, helping to distribute the incompressible yolk toward the ectodermal region. This leads to a slight shortening of the ectoderm. We implement the effects of the yolk in a manner analogous to the constant-volume constraint of individual cells. Specifically, we assign an energy term,  $C_{YOLK}(V_{yolk})$ , in Eq. 1 that is given by the equation

$$C_{YOLK}(V_{yolk}) = K_Y(V_{yolk} - V_{o,yolk})^2 - P_Y V_{yolk} \quad (5)$$

Here,  $V_{yolk}$  is the volume of the yolk and  $V_{o,yolk}$  is the volume of the yolk at equilibrium.  $P_Y$  is the outward isotropic pressure of the yolk. The parameter  $K_Y$  controls the deviations of yolk volume  $V_{yolk}$  from the initial volume,  $V_{o,yolk}$ . We used a value of  $K_Y = 10$ , which limited the maximum change in yolk volume to  $\sim 1\%$ .

The values of parameters  $K_V$  and  $K_Y$  are set high enough to ensure the near constancy of the volumes of individual cells and the yolk. This ensures that the deformation of the cells proceeds exclusively through changes in the geometry of the apical, lateral, and basal surfaces and not through

changes in the volumes of individual cells or that of the yolk. In fact, increasing the values of  $K_V$  and  $K_Y$  beyond  $K_V = 100$  and  $K_Y = 10$  does not change the final model morphology and only increases the total simulation time needed to reach the final state (see section C of the [Supporting Material](#)). Therefore,  $K_V$  and  $K_Y$  do not enter as free parameters into our model.

## SUPPORTING MATERIAL

Ten figures, Supporting Methods, and two movies are available at [http://www.biophysj.org/biophysj/supplemental/S0006-3495\(14\)00730-9](http://www.biophysj.org/biophysj/supplemental/S0006-3495(14)00730-9).

## SUPPORTING CITATIONS

References (42–45) appear in the [Supporting Material](#).

## REFERENCES

- Leptin, M. 2005. Gastrulation movements: the logic and the nuts and bolts. *Dev. Cell.* 8:305–320.
- Holtfreter, J. 1943. A study of the mechanics of gastrulation. Part 1. *J. Exp. Zool.* 94:261–318.
- Gustafson, T., and L. Wolpert. 1962. Cellular mechanisms in the morphogenesis of the sea urchin larva. Change in shape of cell sheets. *Exp. Cell Res.* 27:260–279.
- Quintin, S., C. Gally, and M. Labouesse. 2008. Epithelial morphogenesis in embryos: asymmetries, motors and brakes. *Trends Genet.* 24:221–230.
- Lecuit, T., and P. F. Lenne. 2007. Cell surface mechanics and the control of cell shape, tissue patterns and morphogenesis. *Nat. Rev. Mol. Cell Biol.* 8:633–644.
- Leptin, M. 1995. *Drosophila* gastrulation: from pattern formation to morphogenesis. *Annu. Rev. Cell Dev. Biol.* 11:189–212.
- Costa, M., E. T. Wilson, and E. Wieschaus. 1994. A putative cell signal encoded by the folded gastrulation gene coordinates cell shape changes during *Drosophila* gastrulation. *Cell.* 76:1075–1089.
- Martin, A. C., M. Kaschube, and E. F. Wieschaus. 2009. Pulsed contractions of an actin-myosin network drive apical constriction. *Nature.* 457:495–499.
- Martin, A. C. 2010. Pulsation and stabilization: contractile forces that underlie morphogenesis. *Dev. Biol.* 341:114–125.
- Martin, A. C., M. Gelbart, ..., E. F. Wieschaus. 2010. Integration of contractile forces during tissue invagination. *J. Cell Biol.* 188:735–749.
- Roh-Johnson, M., G. Shemer, ..., B. Goldstein. 2012. Triggering a cell shape change by exploiting preexisting actomyosin contractions. *Science.* 335:1232–1235.
- Kam, Z., J. Minden, ..., M. Leptin. 1991. *Drosophila* gastrulation: analysis of cell shape changes in living embryos by 3-dimensional fluorescence microscopy. *Development.* 112:365–370.
- Leptin, M., and B. Grunewald. 1990. Cell shape changes during gastrulation in *Drosophila*. *Development.* 110:73–84.
- Sweeton, D., S. Parks, ..., E. Wieschaus. 1991. Gastrulation in *Drosophila*: the formation of the ventral furrow and posterior midgut invaginations. *Development.* 112:775–789.
- Thisse, B., C. Stoetzel, ..., F. Perrin-Schmitt. 1988. Sequence of the *twist* gene and nuclear localization of its protein in endomesodermal cells of early *Drosophila* embryos. *EMBO J.* 7:2175–2183.
- Wyczalkowski, M. A., Z. Chen, ..., L. A. Taber. 2012. Computational models for mechanics of morphogenesis. *Birth Defects Res. C Embryo Today. Rev.* 96:132–152.
- Rauzi, M., A. Hočevár Brezavčiček, ..., M. Leptin. 2013. Physical models of mesoderm invagination in *Drosophila* embryo. *Biophys. J.* 105:3–10.

18. Odell, G. M., G. Oster, ..., B. Burnside. 1981. The mechanical basis of morphogenesis. I. Epithelial folding and invagination. *Dev. Biol.* 85:446–462.
19. Pouille, P. A., and E. Farge. 2008. Hydrodynamic simulation of multicellular embryo invagination. *Phys. Biol.* 5:015005.
20. Muñoz, J. J., K. Barrett, and M. Miodownik. 2007. A deformation gradient decomposition method for the analysis of the mechanics of morphogenesis. *J. Biomech.* 40:1372–1380.
21. Conte, V., F. Ulrich, ..., M. Miodownik. 2012. A biomechanical analysis of ventral furrow formation in the *Drosophila melanogaster* embryo. *PLoS ONE.* 7:e34473.
22. Conte, V., J. J. Muñoz, and M. Miodownik. 2008. A 3D finite element model of ventral furrow invagination in the *Drosophila melanogaster* embryo. *J. Mech. Behav. Biomed. Mater.* 1:188–198.
23. Conte, V., J. J. Muñoz, ..., M. Miodownik. 2009. Robust mechanisms of ventral furrow invagination require the combination of cellular shape changes. *Phys. Biol.* 6:016010.
24. Brodland, G. W., V. Conte, ..., M. Miodownik. 2010. Video force microscopy reveals the mechanics of ventral furrow invagination in *Drosophila*. *Proc. Natl. Acad. Sci. USA.* 107:22111–22116.
25. Brodland, G. W., D. Viens, and J. H. Veldhuis. 2007. A new cell-based FE model for the mechanics of embryonic epithelia. *Comput. Methods Biomech. Biomed. Engin.* 10:121–128.
26. Allena, R., A.-S. Mournival, and D. Aubry. 2010. Simulation of multiple morphogenetic movements in the *Drosophila* embryo by a single 3D finite element model. *J. Mech. Behav. Biomed. Mater.* 3:313–323.
27. Hočevár Brezavšček, A., M. Rauzi, ..., P. Zihler. 2012. A model of epithelial invagination driven by collective mechanics of identical cells. *Biophys. J.* 103:1069–1077.
28. Davidson, L. A., M. A. R. Koehl, ..., G. F. Oster. 1995. How do sea urchins invaginate? Using biomechanics to distinguish between mechanisms of primary invagination. *Development.* 121:2005–2018.
29. Sherrard, K., F. Robin, ..., E. Munro. 2010. Sequential activation of apical and basolateral contractility drives ascidian endoderm invagination. *Curr. Biol.* 20:1499–1510.
30. Hufnagel, L., A. A. Teleman, ..., B. I. Shraiman. 2007. On the mechanism of wing size determination in fly development. *Proc. Natl. Acad. Sci. USA.* 104:3835–3840.
31. Farhadifar, R., J. C. Röper, ..., F. Jülicher. 2007. The influence of cell mechanics, cell-cell interactions, and proliferation on epithelial packing. *Curr. Biol.* 17:2095–2104.
32. Schejter, E. D., and E. Wieschaus. 1993. Functional elements of the cytoskeleton in the early *Drosophila* embryo. *Annu. Rev. Cell Biol.* 9:67–99.
33. Fyrberg, E. A., and L. S. B. Goldstein. 1990. The *Drosophila* cytoskeleton. *Annu. Rev. Cell Biol.* 6:559–596.
34. Gilden, J., and M. F. Krummel. 2010. Control of cortical rigidity by the cytoskeleton: emerging roles for septins. *Cytoskeleton (Hoboken).* 67:477–486.
35. Manning, A. J., K. A. Peters, ..., S. L. Rogers. 2013. Regulation of epithelial morphogenesis by the G protein-coupled receptor mist and its ligand fog. *Sci. Signal.* 6:ra98.
36. Gelbart, M. A., B. He, ..., M. Kaschube. 2012. Volume conservation principle involved in cell lengthening and nucleus movement during tissue morphogenesis. *Proc. Natl. Acad. Sci. USA.* 109:19298–19303.
37. Ziemann, F., J. Rädler, and E. Sackmann. 1994. Local measurements of viscoelastic moduli of entangled actin networks using an oscillating magnetic bead micro-rheometer. *Biophys. J.* 66:2210–2216.
38. Zagar, G., P. R. Onck, and E. van der Giessen. 2011. Elasticity of rigidly cross-linked networks of athermal filaments. *Macromolecules.* 33:7026–7033.
39. Dennerll, T. J., P. Lamoureux, ..., S. R. Heidemann. 1989. The cytomechanics of axonal elongation and retraction. *J. Cell Biol.* 109:3073–3083.
40. Kölsch, V., T. Seher, ..., M. Leptin. 2007. Control of *Drosophila* gastrulation by apical localization of adherens junctions and RhoGEF2. *Science.* 315:384–386.
41. Dawes-Hoang, R. E., K. M. Parmar, ..., E. F. Wieschaus. 2005. Folded gastrulation, cell shape change and the control of myosin localization. *Development.* 132:4165–4178.
42. Parks, S., and E. Wieschaus. 1991. The *Drosophila* gastrulation gene *concertina* encodes a G alpha-like protein. *Cell.* 64:447–458.
43. Gregor, T., W. Bialek, ..., E. F. Wieschaus. 2005. Diffusion and scaling during early embryonic pattern formation. *Proc. Natl. Acad. Sci. USA.* 102:18403–18407.
44. Strange, K. 2004. Cellular volume homeostasis. *Adv. Physiol. Educ.* 28:155–159.
45. Nocedal, J., and S. J. Wright. 2006. Numerical Optimization, 2nd ed. Springer Science, New York.